Confusion noise in SPIRE surveys
Version 0.2

H. Aussel, L. Vigroux, P. André
Service d'Astrphysique, CE-Saclay, DSM/DAPNIA,
Bat 709, Orme des Merisiers, CE-Saclay,
F-91191 Gif-sur-Yvette *Cedex*

November 30, 1998

Abstract

We present a simplificated model of extragalactic surveys with SPIRE, the Spectral and Photometric Imaging REceiver on board of FIRST, performed at 250 μm and 500 μm, in order to study the impact of confusion noise. We show on preliminary simulations that confusion is the major issue for dealing with extragalactic source extraction.

Note : Some of the remarks of the note of the 26 October 1998 by Griffin, Oliver and Gear have been taken ino account.

Introduction

This report address the problem of confusion noise for SPIRE, the FIRST bolometer instrument, for its survey mode. Indeed, confusion could be the main limitation of the instrument, due to the high number of extragalactic sources per square arc degree that are predicted by various number counts models. In order to investigate the problem of confusion, we have developped a very simplificated model of a SPIRE survey and we have simulated observations at 250 μm and 500 μm with two kind of detectors : square pixel matrix of bolometers and array of horns (back-up option). We describe in section 1 the model we have used.

1 The model.

1.1 Model for source fluxes and positions

To model the sky as observed in SPIRE surveys, we have used two of number counts models presented in [1], namely the number counts model of Franceschini et al. (1997) [2], and the one of Rowan-Robinson (1998) [4], because they are two extreme models from the point of view of the predicted source density, the counts predicted by the model developped by Guiderdoni et al. (1998) [3] lay between the values predicted by the two others.

Each model result is a function that gives the number N of sources brigther than a given flux S per square degree as a fuction of S. The derivative of this function $N(>S)$ is the number of sources dN with a flux $s \in [S, S+dS]$, multiplied by a factor -1. If one consider only a given flux range, $[S_l, S_u]$, one can build a function f, that gives the number of sources per square degree *dimmer* than a given flux S

and brighter than S_l :

$$f(S) = \int_{S_l}^{S} dN(s)ds \tag{1}$$

If one consider now the function $F(S)$ defined by :

$$F(S) = \begin{cases} 0 & \text{if } S < S_l, \\ \frac{f(S)}{f(S_u)} & \text{if } S_l < S < S_u, \\ 1 & \text{if } S > S_u. \end{cases} \tag{2}$$

The function F grows from 0 to 1 when S varies between $]-\infty, +\infty[$. In this sense, $F(S)$ can be interpreted as the *partition function* of the random variable X_S, the flux of a source. We can therefore build a random flux generator, that follows the number counts model, by computing the function F and using the classical computer implemented uniform generator. The random variable $X = F^{-1}(U)$, where U is a random variable following the uniform law, will have F as partition function.

To simulate a given area of sky A, the models predict that the number of sources brighter than S_l will be $n = A \times N(> S_l)$. We work on an area large enough so that poissonian fluctuations ($\propto 1/\sqrt{n}$) can be neglected.

We choose to simulate an area of 400 square arc minutes, where the number of sources brighter than 15 mJy is roughly of 130, according to the Franceschini model. For our simulations, we choose $S_l = 100\ \mu Jy$ and $S_u = 10\ Jy$. This S_l value gives a number N of sources in our simulation of 16746, with the Franceschini model, $N = 6822$ with the Rowan-Robinson model.

The fluxes of the sources are generated with our random flux generator. The counts obtained from the simulated sets are shown in figure 1 for the various models. The positions in the images are generated by using a uniform generator.

1.2 Simulation of the focal plane

Once the positions and fluxes of the sources are known, we compute a oversampled image of the focal plane of FIRST. The resolution choosed for the computations is 0.5 arcsec, allowing for a good accuracy of the computations, since the smallest pixel size of SPIRE to be considered is 9 arcsec.

We assume an ideal telescope *i.e.* a single circular aperture. Therefore, the intensity of the diffraction limited image of a point source (PSF) is :

$$I = I_0 \left[\frac{J_1(m)}{m}\right]^2 \tag{3}$$

where J_1 is the Bessel function and with :

$$m = \frac{\pi a i}{\lambda} \tag{4}$$

where a is the telescope aperture ($a = 3.5m$), $\lambda = 250\ \mu$m or $\lambda = 509\ \mu$m is the wavelength, and i is the incidence angle (we use the approximation of small angles).

We have computed PSF with a resolution of 0.5 arcsec on the focal plane, on an area of 240 × 240 arcsec. An image of 20 × 20 arcmin with a resolution of 0.5 arcsec is computed by adding one PSF multiplied by the flux for each sources.

Figure 2 presents two simulated fields from each of the two models used.

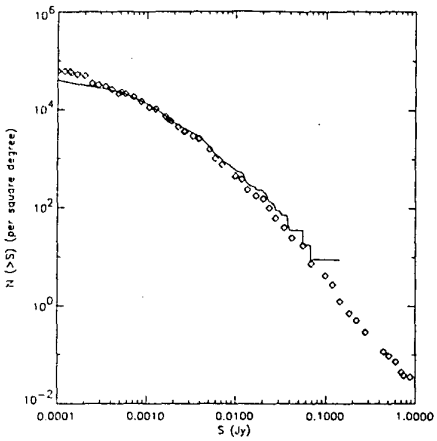

(a) $\lambda = 250$ μm counts model from Rowan-Robinson (1998)[4]

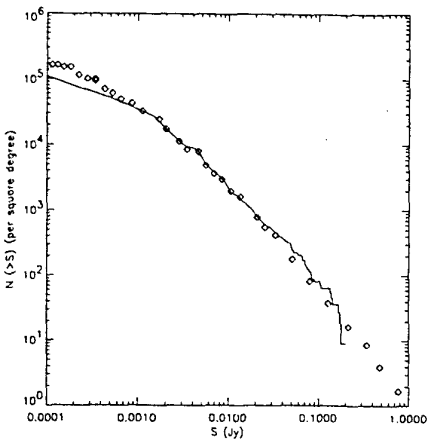

(b) $\lambda = 250$ μm counts model from Franceschini et al. (1997)[2]

Figure 1: Comparaison of the counts obtained with the simulated fluxes with the models.
Line : counts derived from the simulation of a 400 arcmin area.
Diamonds : predictions of the model

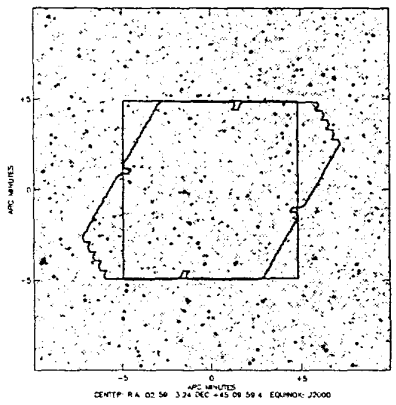

(a) $\lambda = 250$ μm counts model from Franceschini et al. (1997)[2]. Upper cut is 0.2 mJy/arcsec^2.

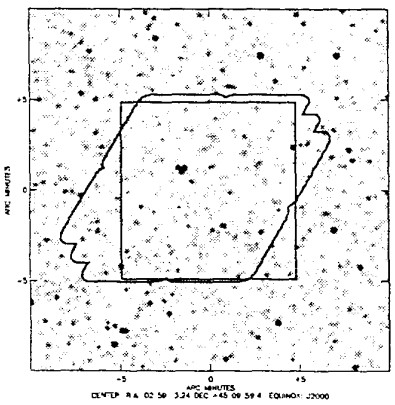

(b) $\lambda = 500$ μm counts model from Franceschini et al. (1997)[2]. Upper cut is 0.1 mJy/arcsec^2.

Figure 2: Simulated images of a 20 × 20 arcmin area of the sky, as observed at the focus of FIRST telescope at 250 μm with a resolution of 0.5 arcsec. The images are displayed with a resolution of 2 × 2 arcsec. At 500 μm, confusion is already a problem for faint fluxes with the Franceschini et al. (1997) [2] model (b) at the resolution of the display, that is four times broader than the resolution of the computations. The area surveyed with option 1 and 2 (squares) and option 3 are outlined.

Option	λ_{obs}	Pixel size	Number of pixels
1 ($F\lambda$)	250 μm	18"	16 × 16
	500 μm	36"	8 × 8
2 ($F\lambda/2$)	250 μm	9"	32 × 32
	500 μm	18"	16 × 16
3 ($2F\lambda$)	250 μm	36"	61
	500 μm	72"	19

Table 1: Detailed parameter of the detectors.

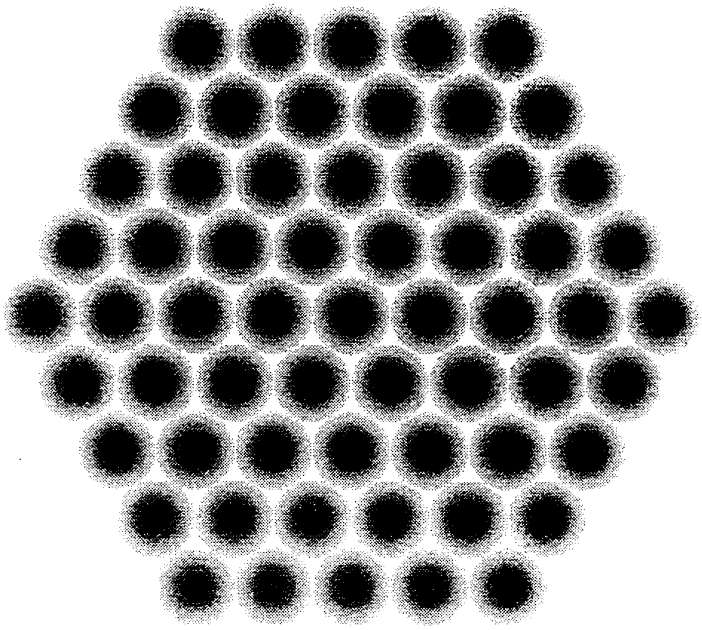

Figure 3: Image of the response of the 61 horns bolometers array

1.3 Simulation of the detectors

We have considered three kind of detectors summarized in table 1 :

1. array of 16×16 square pixels of $F\lambda$ of size, *i. e.* 18 arcsec at 250 μm, and 8×8 pixels of 36 arcsec at 500 μm. The pixels are contigous and their response is constant over the whole pixel.

2. array of 32 × 32 square pixels of $F\lambda/2$ of size, *i. e.* 9 arcsec at 250 μm, and 16 × 16 pixels of 18 arcsec at 500 μm.. The pixels are contigous and their response is constant over the whole pixel.

3. array of 61 bolometers horns (backup option). The horns hexagonaly placed and separated by $2F\lambda$. Their response is a gaussian of $F\lambda$ FWHM. Figure 3 present a image of the array response.

The calculated image of the survey is projected on the detector, to simulate each pointing of the raster for cases 1 and 2, or of a jiggling map for case 3.

In SPIRE, we have taken two sources of noise into account :

1. detector noise with Noise Equivalent Power (NEP) equal to [1] : $NEP_{det} = 3 \times 10^{-17} W.Hz^{-1/2}$

2. photon noise NEP_{ph}, that is dominated by the telescope itself.

The photon Noise Equivalent Power is computed from the RMS fluctuation $(\Delta n)^2$ of the number n of photon of a black body that arrive on the detector [5]. Thus we have:

$$(\Delta n)^2 = n(n+1) \tag{5}$$

The photon emission is dominated by the telescope, with emissivity ϵ and temperature $T = 80$ K [1]. Last, this energy is received by a bolometer with quantum efficiency η_{bol}, with a telescope of collecting collecting area A_t seeing the pupil under the solid angle Ω, in the frequency range $\Delta\nu$, through an optic with efficiency η_{opt}.The fluctuation of the number N of photon arriving on the detector is therefore :

$$(\Delta N)^2 = \epsilon\eta_{bol}\eta_{opt}N(1+\epsilon\eta_{bol}\eta_{opt}N) = \frac{\epsilon\eta_{bol}\eta_{opt}}{e^{\frac{h\nu}{kT}}-1}\left(\frac{\epsilon\eta_{bol}\eta_{opt}}{e^{\frac{h\nu}{kT}}-1}+1\right) \tag{6}$$

Each photon has an energy $h\nu$ and the density of states it can occupy is :

$$d = 2 \times \frac{2h\nu^3}{c^2} \tag{7}$$

Therefore we have :

$$NEP_{ph}^2(\lambda) = A_t\Omega \int_{\Delta\nu} 2 \times \frac{2h\nu^3}{c^2}(h\nu)\frac{\epsilon\eta_{bol}\eta_{opt}}{e^{\frac{h\nu}{kT}}-1}\left(\frac{\epsilon\eta_{bol}\eta_{opt}}{e^{\frac{h\nu}{kT}}-1}+1\right)d\nu \tag{8}$$

We have for SPIRE [1] :

$$A_t\Omega = \alpha\lambda^2 \qquad T_{tel} = 80K \qquad \epsilon_{tel} = 0.04 \tag{9}$$

$$\eta_{opt} = 0.3 \qquad \eta_{bol} = 0.8 \qquad \Delta\lambda = \frac{\lambda}{3} \tag{10}$$

The value of α depends on the configuration, taking into account Lyot spot and area of the bolometer. Following [6], we take for option 3 $\alpha = 0.8$ so that $A_3\Omega_3 = 0.8\lambda^2$. For square pixels, $\Omega = \pi/4F^2$ [6] is the same (the telescope has the same optical configuration) and the collecting area are $A_1 = (F\lambda)^2$ and $A_2 = (F\lambda)^2/4$, where F is the focal length of the telescope.

The total noise equivalent power of the bolometer NEP_{tot} is then :

$$NEP_{tot} = \sqrt{NEP_{ph}^2 + NEP_{det}^2} \tag{11}$$

If one observes a point source radiating with the flux density $S_{\nu,s}$, assumed to be constant over $\Delta\nu$, the bolometer receives the power :

$$P_b = S_{\nu,s}\, A_t\, \Delta\nu\, \eta_{tel+det}\, \eta_{pix} \tag{12}$$

where η_{pix} is the portion of the PSF intercepted by the bolometer, $\eta_{tel+det}$ is the overall efficiency of the instrument and telescope. We have :

$$\eta_{tel+det} = \eta_{opt}\, \eta_{bol}\, \eta_{chop} \tag{13}$$

		option 1 $\alpha = \pi/4 = 0.785$	option 2 $\alpha = \pi/16 = 0.196$	option 3 $\alpha = 0.8$
Wavelength	Noise	NEP $(10^{-17} W.Hz^{-1/2})$	NEP $(10^{-17} W.Hz^{-1/2})$	NEP $(10^{-17} W.Hz^{-1/2})$
250 μm	photon	9.06	4.53	9.14
	detector	3.00	3.00	3.0
	total	9.54	5.43	9.62
500 μm	photon	5.05	2.53	5.10
	detector	3.00	3.00	3.00
	total	5.88	3.92	5.92
Wavelength	Noise	r.m.s. (mJy)	r.m.s. (mJy)	r.m.s. (mJy)
250 μm	total	0.63	0.36	0.63
500 μm	total	0.77	0.52	0.78

Table 2: Noise equivalent power and noise level (1 σ/pixel) for simulation of 15 min exposures.

where $\eta_{chop} = 0.45$ is the chopping efficiency and $A_t = \pi 3.29^2/4$ [1].

If this sources is observed during the time t, the noise reduces as $\sqrt{t}$ and the signal over noise ratio is therefore :

$$S/N = \frac{S_{\nu,s}\, A_t\, \Delta\nu\, \eta_{tel+det}\, \eta_{pix}}{\frac{NEP_{tot}}{\sqrt{2\,\eta_{obs}\, t}}} \tag{14}$$

Note that the observing time has been multiplied by a factor η_{obs}, the observation efficiency, to take into account the overheads *i. e.* that not all the time dedicated to the observation is used to take data.

The equation 14 allow to compute the signal over noise for the detection of a point source. In our case, we are interested in computing the noise level in one pixel. Thus, we have to consider for this purpose the observatiom of a constant extended source and use the following equation :

$$S/N = \frac{S_{\nu,s}\, A_t\, \Delta\nu\, \eta_{tel+det}}{\frac{NEP_{tot}}{\sqrt{2\,\eta_{obs}\, t}}} \tag{15}$$

where η_{pix}, the pixel efficiency, that is the average flux recieved by a pixel when observing a source, is no longer taken into account.

Setting S/N to 1 in equation 15 gives us the flux density r.m.s. of the noise, which, in this case is equal to $S_{\nu,s}$.

Values of α and NEPs are summarized in table 2. Note that we assume that the noise is independant of the simulated sources, because we assume that photon noise due to the sources is neglictible against those of the background and telescope.

Once the projection of one pointing (raster step or jiggling step) has been computed, a gaussian noise with r.m.s. corresponding to the option and wavelength is added to the image.

1.4 Map reconstruction

Once each image (*i.e.* the flux collected by each bolometer for a given pointing) has been computed, they are coadded in a "raster" or "jiggle" map. We follow for this

the prescriptions of the IRAM reduction package NIC [7]. Each pointing is added to the raster map with a weight W :

$$W = \left(\frac{\sin(ud)}{ud}\right)^2 T \quad (16)$$

$$u = \frac{2\pi D}{\lambda} \quad (17)$$

where d is the distance between the poition of the final map and the center of the bolometer and T is the value of the transfert function of the bolometer at this point. A noise map is also produced, using W^2 as weight.

The map of the observation is then interpolated on a regular RA-DEC oriented grid using bilinear interpolation. In option 3, where directions of the "jiggling" are not perpendicular, care has been taken to have a flux conservative reprojection.

2 Results

The model described in the previous section has been used to simulate survey observations with the three kind of detectors. Due to SPIRE design the three (of which two are simulated) are observed at the same time. This means that the same pointings and same integration time are used for the two channels. To fully sample the PSF at the longuest wavelength, one has to scan the sky by steps of $\lambda/2$ in both axis. These leads to a scan in only λ for the shortest wavelength thus leading to an undersampled map. Thus the minimal sampling rate is $\lambda/2$ at 250 μm that gives $\lambda/4$ at 500 μm. Together with this minimal sampling, we have simulated oversampled maps at $\lambda/4$ at 250 μm and $\lambda/8$ at 500 μm.

While the shortest wavelength commands the raster or jiggle step size, the longuest wavelength commands the number of steps : the bolometer size has to be fully covered in order to obtain an homogeneous map. If a $\lambda/2$ step at 250 μm requires 4 $\times$ steps to obtain a full coverage of the PSF at 250 μm, this translate to $\lambda/4$ at 500 μm. Thus, a 8 $\times$8 map is in fact required.

2.1 Observations

In order to ensure a proper comparaison of the three detector, we have simulated observations of an area of *fixed surface* within a *fixed total observation time* at a *fixed resolution*. The area for each configuration is $100\,arcmin^2$, except for option 3 (2 Fλ horns) at 500 μm where the 27 horns cover a slightly larger surface giving a total area of $113\,arcmin^2$. To cover at $\lambda/4$ and 250 μm this area, 4 "jiggle" maps of 64 pointings each are required. We set the observing time to 64 minutes, giving an exposure time of 15 seconds per pointings in this configuration. The exposure time per pointing for each other options where computed to fill the same total observing time. For exemple, an array of 16$\times$16 square pixels of 18" can map the same area in the same time and stay 60" at each pointing, with 4 raster maps with half a pixel steps.

The detectors are detailed in table 1 and the observations are detailed in table 3

2.2 Images

Figures 4, 5 and 6 present the images obtained at 250 μm and 500 μm with the low resolution and high resolution mode, on the field simulated with Franceschini et al. number counts [2]. Figures 4, 5 and 6 present the same results for Rowan-Robinson number counts [4]. Note that we had to modify the lower cut of option 3 results

Option	Resolution at 250 μm	Number of pointings	Exposure time	Covered area	Total time
1(Fλ)	$\lambda/2$	4×4×4	1 min	100	1.07
	$\lambda/4$	8×8×4	0.25 min	100	1.07
2 (Fλ/2)	$\lambda/2$	2×2×4	4 min	100	1.07
	$\lambda/4$	4×4×4	1 min	100	1.07
3 (2Fλ)	$\lambda/2$	8×8×4	0.25 min	100	1.07
	$\lambda/4$	16×16×4	0.0625 min	100	1.07

Table 3: Details of the simulated observations. For each option, the step size (resolution) at 250 μm is given, as well as the number of pointing required for a complete coverage at 500 μm. The number of pointings is given in the following way : $N_{step_1} \times N_{step_2} \times N_{raster}$ where N_{raster} is the number of independant raster or jiggle maps needed to cover the area.

to leave some dynamics in the image. Indeed, lower cut is 10 σ while it is 1 σ for options 1 and 2.

It is clear from the output images that confusion dominates all the maps for source extraction. With option 3 (2Fλ horns), only a few pixels are below the 1 σ level, at the edge of the map where redundancy is small, and most of the pixel are *above* the usual 3 σ level used for source détection. Moreover, many sources appear blended together, whatever the detector being used.

Depending on the kind of observations and the detector, the effects of confusion are more or less severe :

- The mapped obtained at a better resolution are less affected.
- The smaller the pixels, the less prominent is confusion at high flux level.

When dealing with exposures as long as the ones simulated, the detector and photon noise originating from the telescope mirror become neglictibles, especially for large pixels.

Two ways can be though to overcome the confusion problem :

- use pixels as small as possible to fight this effect, but big enough to avoid to be dominated by instrument noise.
- observe with scan maps rather than pointed "jiggle" maps, in order to obtain a high resolution on the final map. This is only possible if the relative pointing accuracy and control of the satellite is good.

Two techniques are usually used detect sources against confusion : the deconvolution and the P(D) analysis. Both require a good understanding of the instrumental noise, as well as accurate measures of the beam profile, that are difficult to obtain, especially when the the intrument is very sensitive.

3 Conclusion

We have presented a simplificated model of extragalactic surveys with SPIRE, the Spectral and Photometric Imaging REceiver on board of FIRST, performed at 250 μm and 500 μm, in order to study the impact of confusion noise. We show on preliminary simulations that confusion is the major issue for dealing with extragalactic source extraction. We show that a detector made of small pixel (Fλ/2) is

less sensitive to this problem. Observations obtained with very small steps between pointings or scan technique are also preferred.

Beyond the scope of extragalactic surveys, the problem rises the question of finding a good "empty" place when using chopping techniques. The probability of finding a source bright enough to be above the noise level for in any part of the sky is large, even for short exposures.

This study will be extended to take into detectors closer to reality : non homogenous response of the pixels, pixels with filling factor lower than one, *etc...* Moreover, tests of P(D) and deconvolution will be done to analyse the outputs of the simulations.

References

[1] Griffin M., and the SPIRE consortium, 1998, "SPIRE, a bolometer instrument for FIRST", A proposal to the European Space Agency

[2] Franceschini A., Aussel H., Bressan A. *et al.*, 1997, "Sources counts and background radiation", in *The Far Infrared and Submillimeter Universe*, ESA SP-401

[3] Guiderdoni B., Hivon E., Bouchet F., Maffei B., 1998, MNRAS, 295,877

[4] Rowan-Robinson M., 1998, MNRAS *in press*

[5] Rohlfs K., Wilson L. T., 1996, "Tools of Radio Astronomy", second edition, Springer

[6] Griffin M., Bock J., Gear W., "Comparison of sensitivities of 0.5Fλ, 1.0Fλ and 2.0Fλ arrays for the BOL", Note no. BOL/QMW/N/0026.10

[7] D.Broguière, R.Neri, A.Sievers, NIC Bolometer Users Guide, Version 1.4-01, *http://iraux2.iram.fr/GS/nic/nic.html*

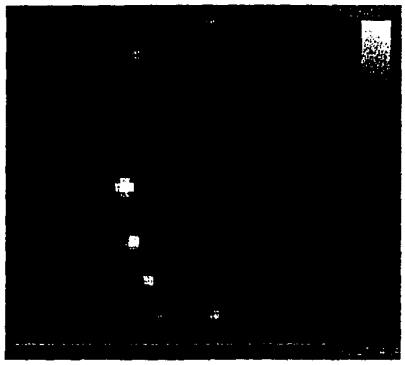

(a) $\lambda = 250$ μm, resolution of $\lambda/2$. Display is Log(f mJy/pixel). Lower cut is 1σ, upper cut is 20 σ.

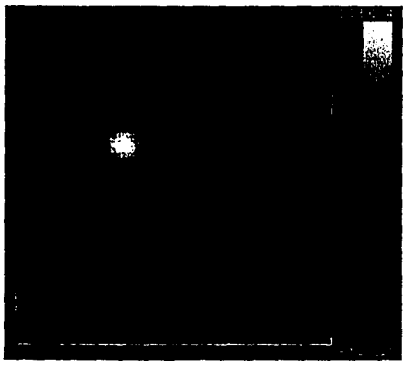

(b) $\lambda = 500$ μm, resolution of $\lambda/4$. Display is Log(f mJy/pixel). Lower cut is 1σ, upper cut is 40 σ.

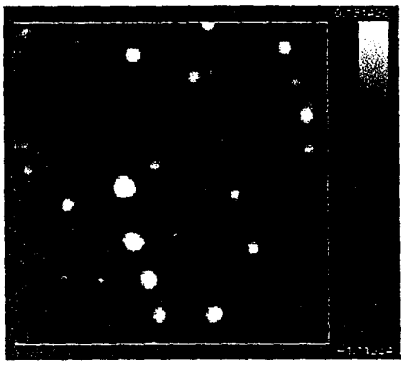

(c) $\lambda = 250$ μm, resolution of $\lambda/4$. Display is Log(f mJy/pixel). Lower cut is 1σ, upper cut is 20 σ.

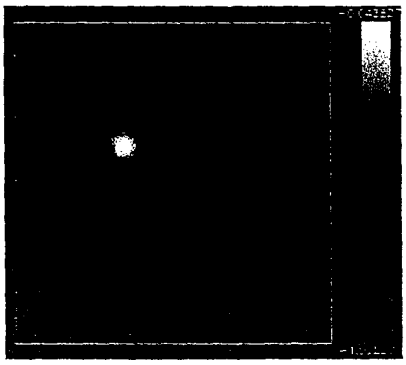

(d) $\lambda = 500$ μm, resolution of $\lambda/8$. Display is Log(f mJy/pixel). Lower cut is 1σ, upper cut is 40 σ.

Figure 4: Observation with option 1 (Fλ square pixels), with a final resolution of $\lambda/2$ at 250 μm (panels a and b), and with a final resolution of $\lambda/4$ at 250 μm (panels c and d)

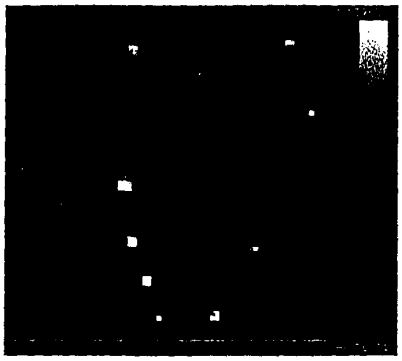

(a) $\lambda = 250$ μm, resolution of $\lambda/2$. Display is Log(f mJy/pixel). Lower cut is 1σ, upper cut is 40 σ.

(b) $\lambda = 500$ μm, resolution of $\lambda/4$. Display is Log(f mJy/pixel). Lower cut is 1σ, upper cut is 80 σ.

(c) $\lambda = 250$ μm, resolution of $\lambda/4$. Display is Log(f mJy/pixel). Lower cut is 1σ, upper cut is 40 σ.

(d) $\lambda = 500$ μm, resolution of $\lambda/8$. Display is Log(f mJy/pixel). Lower cut is 1σ, upper cut is 80 σ.

Figure 5: Observation with option 2 (F$\lambda/2$ square pixels), with a final resolution of $\lambda/2$ at 250 μm (panels a and b), and with a final resolution of $\lambda/4$ at 250 μm (panels c and d)

(a) $\lambda = 250$ μm, resolution of $\lambda/2$. Display is Log(f mJy/pixel). Lower cut is 10σ, upper cut is 400 σ.

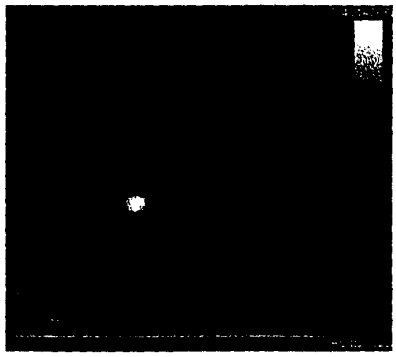

(b) $\lambda = 500$ μm, resolution of $\lambda/4$. Display is Log(f mJy/pixel). Lower cut is 10σ, upper cut is 800 σ.

(c) $\lambda = 250$ μm, resolution of $\lambda/4$. Display is Log(f mJy/pixel). Lower cut is 10σ, upper cut is 400 σ.

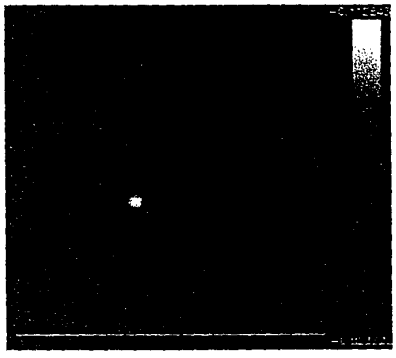

(d) $\lambda = 500$ μm, resolution of $\lambda/8$. Display is Log(f mJy/pixel). Lower cut is 10σ, upper cut is 800 σ.

Figure 6: Observation with option 3 (2Fλ horns), with a final resolution of $\lambda/2$ at 250 μm (panels a and b), and with a final resolution of $\lambda/4$ at 250 μm (panels c and d)